Journal of Marine Systems 74 (2008) 585–591

Contents lists available at ScienceDirect

Journal of Marine Systems

journal homepage: www.elsevier.com/locate/jmarsys

On the influence of large wind farms on the upper ocean circulation

Göran Broström

Norwegian Meteorological Institute, Postboks 43 Blindern, N-0313 OSLO, Norway

ARTICLE INFO

Article history:
Received 21 May 2007
Received in revised form 25 April 2008
Accepted 2 May 2008
Available online 15 May 2008

Keywords:
Wind farm
Wind forcing
Upwelling
Ocean dynamics

ABSTRACT

Large wind farms exert a significant disturbance on the wind speed in the vicinity of the installation and in this study we outline the oceanic response to the wind wake from a large wind farm placed in the ocean. We find that the size of the wind wake is an important factor for the oceanic response to the wind farm. We show through simple analytical models and idealized numerical experiments that a wind speed of 5–10 m/s may generate upwelling/downwelling velocities exceeding 1 m/day if the characteristic width of the wind wake is of the same size or larger than the internal radius of deformation. The generated upwelling is sufficiently enough that the local ecosystem will most likely be strongly influenced by the presence of a wind farm.

© 2008 Elsevier B.V. All rights reserved.

1. Introduction

It is predicted that large open-water wind farms will become much more frequent in the decades to come (Archer and Jacobson, 2003, 2005; Henderson et al., 2003; Kooijman et al., 2003; Hasager et al., 2006). There are certain advantages with oceanic wind farms, not least the higher wind speeds and locations away from densely populated areas. On the negative side are large costs of establishing and maintaining wind farms out in the open water (Byrne and Houlsby, 2003), wave forces on the structures, disturbance of ship traffic, and environmental effects among others.

Although there are a number of plans and studies for large wind farms in the open ocean the environmental consequence are not well known and much of the literature is in a so called gray form represented by reports, theses etc. Presently, the environmental focus has mainly been on the direct consequences of the solid structures of the wind farm on the oceanic environment. The establishment of solid structures will probably act as artificial reefs creating new highly productive areas in the sea. Other possible environmental consequences may be the impact of electric cables on the fish migrations (Branover et al., 1971; Wiltschko and Wiltschko, 1995), effects of sound generated by the power plant on the fauna (Sand and Karlsen, 1986; Karlsen, 1992; Knudsen et al., 1992; Karlsen et al., 2004; Hastings and Popper, 2005), shadowing from the wind mills, and bird and bat collisions with the wind mills (Tucker, 1996a,b; Garthe and Hüppop, 2004; Wiggelinkhuizen et al., 2006). There is probably also an influence of the wind farm on the local climate (Baidya Roy and Pacala, 2004; Rooijmans, 2004) as well as on the global climate if wind farms become abundant (Keith et al., 2004).

In this study we outline how the presence of a large wind farm, which changes the wind stress at the sea surface, affects the upper ocean response to wind forcing. Using general theoretical arguments we show that large wind farms may have a direct, and strong, impact on the circulation pattern around the installation. In particular, if the wind farm is large enough variations in the wind will create upwelling and downwelling patterns around the wind farm through divergence in the Ekman transport. The main theoretical description is based on the so called reduced gravity model, which describes the dynamics of a buoyant layer on top of a dense stagnant layer. The theoretical framework follows standard derivations used in the geophysical fluid dynamics (Gill, 1982; Pedlosky, 1987) and the analysis shows that the oceanic response is more sensitive to the curl of the wind stress than to the wind stress itself. In the open ocean, the curl of the wind stress is usually relatively small as the gradients in the wind forcing are set by the scale of atmospheric low-pressure systems, which are much larger than the corresponding dynamical scales of the ocean. The presence of a wind farm

E-mail address: goran.brostrom@met.no.

0924-7963/$ – see front matter © 2008 Elsevier B.V. All rights reserved.
doi:10.1016/j.jmarsys.2008.05.001

will generate an unnaturally strong horizontal shear in the wind stress, which creates a large curl of the wind stress that causes a divergence/convergence in the upper ocean. We find that the impact on the ocean currents will increase with the size of the wind farm, and when the size is comparable with the internal radius of deformation (or internal Rossby radius) we expect to find a circulation, and an associated upwelling pattern, to be excited by the wind farm. Using a simple example we show that a wind speed of 5–10 m/s can induce an upwelling exceeding 1/m day. It is well known that upwelling can have significant impact on the local ecosystem (e.g., Okkonen and Niebauer, 1995; Valiela, 1995; Botsford et al., 2003; Dugdale et al., 2006). Thus, as upwelling of nutrient rich deep water represent the main source of nutrients during summer in most oceanic areas it is likely that the upwelling induced by a wind farm will imply an increased primary production, which may affect the local ecosystem.

There are some notable similarities between the proposed upwelling process and some natural upwelling systems generated by divergence in the Ekman transport due to wind curls at coastal boundaries (Dugdale et al., 2006; Fennel and Lass 2007) or the marginal ice zone (MIZ) (Røed and O'Brian, 1983; Okkonen and Niebauer, 1995; Fennel and Johannessen, 1998). For the present scenario, the MIZ studies are probably most relevant: Røed and O'Brian (1983) estimated upwelling velocities of order 5 m/day for reasonable wind speeds while Okkonen and Niebauer (1995) invoked upwelling velocities of up to 8 m/day, which were seen to fuel an extensive bloom in the MIZ.

In Section 2, the basic equations that describe the structure of the oceanic response to wind forcing in the vicinity of a wind farm are outlined. Some dynamical features of these equations are described in Section 3, while Section 4 is devoted to discussion of the results.

2. Basic equations

In this section we will outline some simple equations that describe a buoyant surface layer on top of a stagnant deep layer; these equations are very similar to the equations describing the barotropic flow and are generally referred to as the reduced gravity model, or a 1 1/2 layer model. The model is based on integration over the active upper layer and is thus two-dimensional; vertical velocity is manifested as a vertical movement of the pycnocline and is thus included implicitly. It should be remembered that certain conditions must be fulfilled for the reduced gravity model to be valid; the reasonableness of these assumptions can be questioned for the outlined scenarios. However, the reduced gravity model highlights a number of processes that may be important in the vicinity of large wind farms, and the primary aim of the present study is to outline the basic response of the upper ocean to a large wind farm, not to describe these processes in detail.

2.1. Form and strength of wind drag

The form and strength of the perturbations in the wind stress is the basic driving mechanism of this study. The wind stresses used in this study are in the *x*-direction and the wind farm creates a disturbance that is strongest in the *y*-direction. We will consider two simple forms of the wind stress: 1) A wind stress that is homogenous in the *x*-direction such that analytical solutions can be found and 2) a wind wind-stress pattern having a more realistic two-dimensional form. The stresses are given by

$$\begin{aligned} \tau_x &= \tau_{x0} - \Delta\tau_x e^{-(2y/L)^2}, \\ \tau_x &= \tau_{x0} - \Delta\tau_x e^{-(2y/(0.8L+0.2x))^2} \quad max \quad \left(e^{-(1-x)/L} x/L, 0\right), \end{aligned} \tag{1a, b}$$

where τ_{x0} is the wind stress outside the influence of the wind farm, $\Delta\tau_x$ reflect the change in the wind stress induced by the wind farm, and L is the characteristic size of the wind farm. For the more realistic scenario we assume that the wind deficit is zero at the upwind end of the wind farm, reaches a maximum at the end of the farm and declines downwind from the farm with a characteristic length scale L. We also assume that the width of the wind deficit increases in the downwind direction, as expected from turbulent mixing and meandering of the wake. The shapes of the proposed wind stresses are shown in Fig. (1), and follow loosely results from recent studies (Barthelmie et al., 2003; Corten and Brand, 2004; Corten et al., 2004; Hegberg et al., 2004; Christiansen and Hasager, 2005; Hasager et al., 2006). However, it should

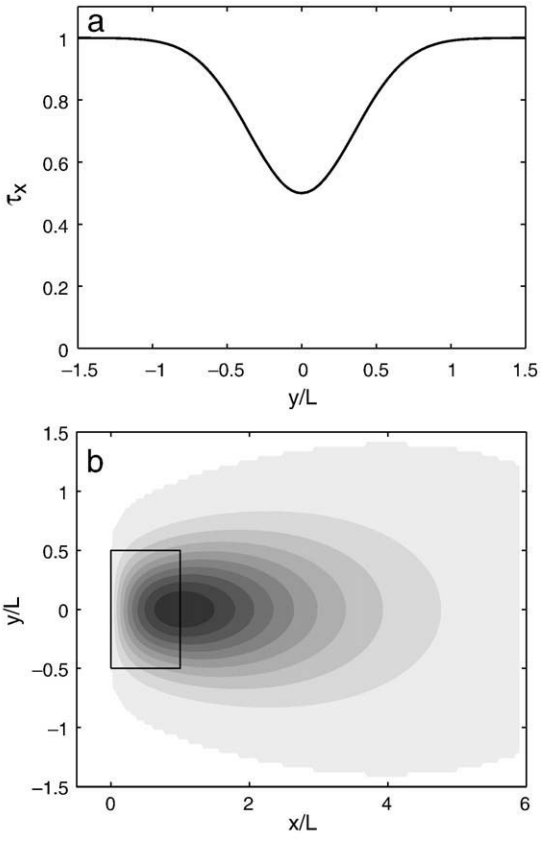

Fig. 1. The wind-stress deficit used in this study. a) Cross section of the one one-dimensional case used for analytical studies and b) map of the more realistic wind-stress deficit, where also the extent of the wind farm is displayed by a black line.

be noted that further investigations focusing on the wind stress at the sea surface are required for more accurate predictions, and specifications, of how a large wind farm influence the wind stress at the sea surface.

2.2. Basic shallow water equations

Let us consider an ocean that rotates with the angular speed $f/2$, where f is the Coriolis parameter, and having an active upper layer with thickness h and density $\rho-\Delta\rho$ overlying an infinitely deep passive layer with density ρ. The horizontal coordinates are x and y; the vertical coordinate is z, which is zero at the sea surface and positive upwards. The bottom of the active layer is located at $z=-h(x,y)$ while the free surface is located at $z=0$ according to the rigid lid approximation (see Fig. 2).

The flow in the active upper layer can be described by integrating the Navier-Stokes and continuity equations from the bottom of the active layer to the surface, and by applying the hydrostatic approximation. Neglecting the non-linear terms for simplicity (although it should be recognized that they are in general not negligible), the linear reduced gravity equations in transport form become

$$\begin{aligned}
&\frac{\partial U}{\partial t}-fV=-g'h_0\frac{\partial h}{\partial x}+\frac{1}{\rho}\tau_x,\\
&\frac{\partial V}{\partial t}+fU=-g'h_0\frac{\partial h}{\partial y}+\frac{1}{\rho}\tau_y,\\
&\frac{\partial h}{\partial t}+\left(\frac{\partial U}{\partial x}+\frac{\partial V}{\partial y}\right)=0,
\end{aligned} \qquad (2a–c)$$

where U and V are the mass transports in x and y directions, respectively, $g'=g\Delta\rho/\rho$ is the reduced gravity, h_0 is the initial thickness of the upper layer and we will assume that $h_0=\text{const}$, τ_x, $\tau_y=(\tau_x^S-\tau_x^B,\tau_y^S-\tau_y^B)$ are the stresses acting on the water column where τ_x^S, τ_y^S, are the surface stresses and τ_x^B, τ_y^B are the stresses at the bottom of the active layer (τ_x^B, τ_y^B are assumed to be zero in this study). An important assumption for the reduced gravity model is that the bottom layer should be deep and stagnant; furthermore, the amplitude in h must be small: These assumptions may be questionable for wind farms placed in relatively shallow water. As a final remark it may seem strange that the gradient of the slope at the lower boundary appears to induce a force in the upper layer; the force comes really from the sloping surface and the slope in the lower layer only removes the pressure gradient from the surface down into the stagnant deep layer. However, the changes in the surface elevation are small and can be neglected in the remaining analysis, and this is the rigid lid approximation.

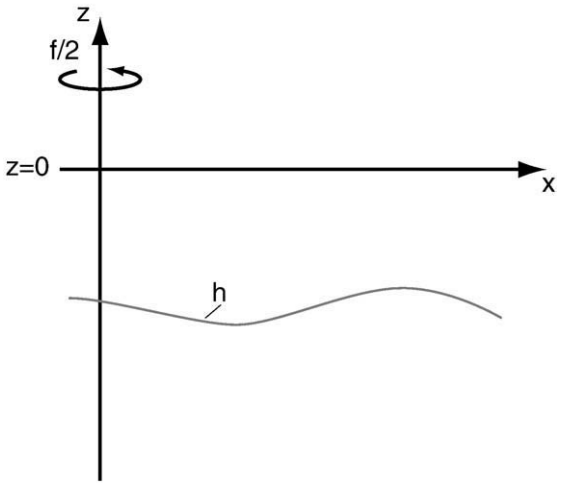

Fig. 2. Schematic picture of the geometric settings used in this study.

2.3. General equation for h

The response of the thickness of the upper layer to wind forcing is the key feature in the reduced gravity model. If the thickness of the upper layer is known, the velocities of the system are easily calculated. After some manipulations of Eq. (2) we find (Gill, 1982; Pedlosky, 1987)

$$\frac{\partial}{\partial t}\left[\left(\frac{\partial^2}{\partial t^2}+f^2\right)h-\nabla\cdot(gh_0\nabla h)\right]=-\frac{f}{\rho}curl(\tau)-\frac{1}{\rho}\frac{\partial}{\partial t}\nabla\cdot\tau. \qquad (3)$$

Eq. (3) is very general and describes an extensive set of phenomena where the reduced gravity approximation is valid. A normal problem in using this equation is to find appropriate boundary conditions (Gill, 1982; Pedlosky, 1987); for the reduced gravity model we will simply assume that $h=h_0$ at the boundaries or that it is bounded at infinity.

In the following analysis we will neglect fast transients such that the second order time derivative in Eq. (3) can be neglected (i.e., we neglect internal gravity waves, the geostrophic adjustment process and all processes for small time $t<f$). Furthermore we assume that the wind forcing is constant and neglect the last term. It is convenient to use non-dimensional variables and we thus introduce the scales $t=t'f^{-1}$, $(x,y)=(x',y')L$, and $h=h'\Delta\tau/f\rho L$: We have (dropping the primes on the non-dimensional variables)

$$\frac{\partial}{\partial t}(h-a^2\nabla^2 h)=-curl\left(\frac{\tau}{\Delta\tau}\right), \qquad (4)$$

where $a=\sqrt{g'h_0}/fL$ is a non-dimensional number (here considered as constant) identified as the internal radius of deformation, or the internal Rossby radius, divided by the size of the wind farm. Eq. (4) is easily integrated in time such that

$$(h-h_0)-a^2\nabla^2(h-h_0)=-tcurl\left(\frac{\tau}{\Delta\tau}\right), \qquad (5)$$

where h_0 is the initial non-dimensional depth of the pycnocline. For the one-dimensional case there exists an analytical solution whereas we solve this equation numerically for two dimensions. The important lesson to be learnt from Eq. (5) is that the depth of the pycnocline changes linearly in time, i.e., $(h-h_0)/t$ has a self-similar solution, and that the rate depends linearly on the strength of the wind-stress curl.

3. Some dynamical features of the equations

3.1. Analytical time-dependent solution for zonal wind forcing

In this section we aim at finding some analytical results. To highlight the ocean response to wind forcing we consider a

wind distribution in the form of a Gaussian, as outlined by Eq. (1a). From Eq. (5) we find that

$$(h-h_0)-a^2\frac{\partial^2}{\partial y^2}(h-h_0)=-t\frac{1}{\Delta\tau_x}\frac{\partial\tau_x}{\partial y}. \tag{6}$$

To obtain the full structure of the solution it is necessary to also solve an inhomogeneous Helmholtz equation. Assuming that the wind stress has a Gaussian distribution (Eq. (1a)), and by requiring that the solution is bounded at infinity we find the following solution

$$\begin{aligned} h(t,y)-h_0 =& t\frac{\sqrt{\pi}}{16a^2}e^{-\frac{1}{8a^2}}\left[e^{\frac{2y}{a}}\left(1-erfc\left(\frac{1}{4a}+2y\right)\right)\right. \\ &\left.-e^{-\frac{2y}{a}}\left(1-erfc\left(\frac{1}{4a}+2y\right)\right)\right] \end{aligned} \tag{7}$$

where erfc is the error function. The disturbance of the upper layer thickness thus increases linearly with time and is proportional to the magnitude of the wake. Due to the dynamics of the geostrophic adjustment process the signal has a form that depends on the non-dimensional parameter a (Fig. 3) (again a is a measure of how large the internal deformation radius is compared to the size of the wind farm). If the variation in wind has a length scale that is much larger than the internal deformation radius the form of the disturbance is fully governed by the form of the wind curl (as seen by setting $a=0$ in Eq. (6)). However, if the structure of the wind field is of the same, or smaller, dimension than the internal deformation radius the ocean responds by distributing the signal over an area with a characteristic width corresponding to the internal deformation radius. It should also be noted that the amplitude of the signal becomes smaller for large values of a^2.

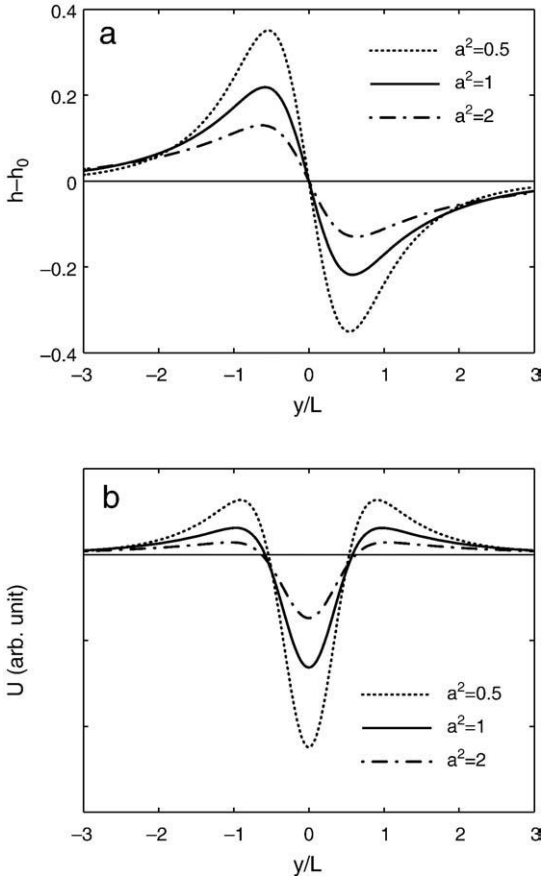

Fig. 3. a) The form of the disturbance in thickness of the upper layer and b) the geostrophic velocity for various number of the a^2 parameter (here the wind forcing is given by $\tau_x=e^{-(2y)^2}$).

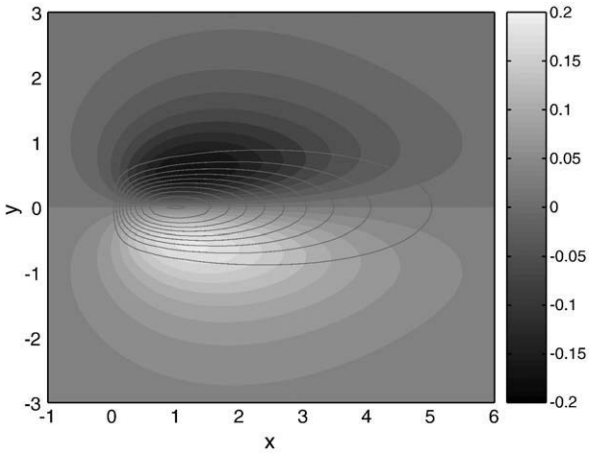

Fig. 4. The spatial structure of the disturbance in thickness of the upper layer for $a^2=1$ and $t=1$. Gray lines represent the wake in the wind forcing.

3.2. More general time-dependent numerical solution

In two dimensions it is more difficult to find analytical solutions and we rely on numerical solutions using the self adapting finite element technique implemented in FEMLAB® package, the relative tolerance was set to 10^{-6} and two refinements of the grid were made (the self adaptation implies that the resolution will depend on the parameter a^2). It should be remembered that the linear solution predicts that the shape of the response is self-similar and will not change in

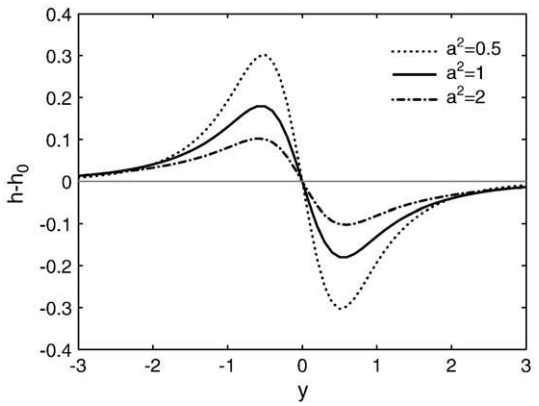

Fig. 5. Section of the disturbance in thickness of the upper layer at the downwind end of the wind farm.

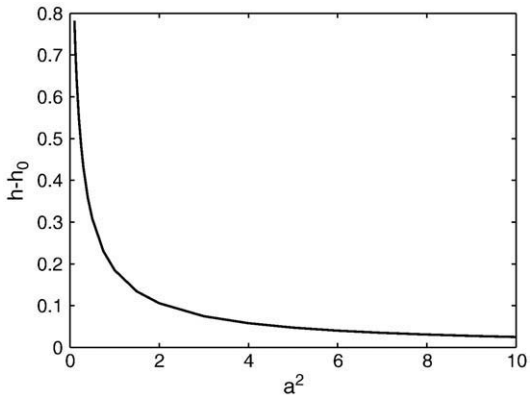

Fig. 6. The maximum amplitude of the disturbance in thickness of the upper layer as a function of a^2.

time and we evaluate the solution at $t=1$ (Fig. 4). From Fig. (5) we see that the pycnocline will rise on the southern side of the wind farm and will be depressed on the northern side. The ocean response follows the wind pattern to a large degree, although the signal covers a slightly larger area than the wind wake as expected from the geostrophic adjustment process.

The spatial response depends critically on the deformation radius, and cross sections of the pycnocline position at $x=1$ (at the downwind end of the wind farm) are displayed in Fig. (5); for $a^2=1$ the amplitude is about 25% of the amplitude for small a^2. Apparently, the geostrophic adjustment process mixes the positive and negative response appearing on each side of the wind wake such that the magnitude of the response becomes weaker. It is a notable feature that the response for increasing value of a^2 becomes wider as well. A key parameter for the environmental influence is the strength of the upwelling and the maximum value of the pycnocline height as a function of a^2 is shown in Fig. (6). Again we see that the amplitude of the response decreases rapidly with a^2, showing that a key parameter for the ocean response is the physical size of the wind wake.

Inserting $f=1.2\cdot10^{-4}$ s^{-1}, $h_0=10$ m, $\Delta\rho=2$ kg/m^3, we find that the internal radius of deformation is 3.7 km and using $L=5$ km we find $a^2\approx0.54$, which implies that there should be an important signal from a 5 km wide wind farm on the upwelling pattern. The upwelling velocity can be estimated from the horizontal shear in the wind wind-stress times the spatial distribution/influence of the response as outlined in Figs. (5) and (6), and we thus expect the maximum upwelling velocity to be roughly $\Delta\tau_x/(\rho fL)\cdot0.3\approx1$ m/day for the case with $\Delta\tau_x=0.025$ N/m^2, and $a^2\approx0.54$. It should be noted that this only gives a very rough estimate of the upwelling velocity. When the disturbances grow larger it is expected that non-linear terms, lower-layer motions, and bottom friction become important. Anyway, the predicted upwelling velocity

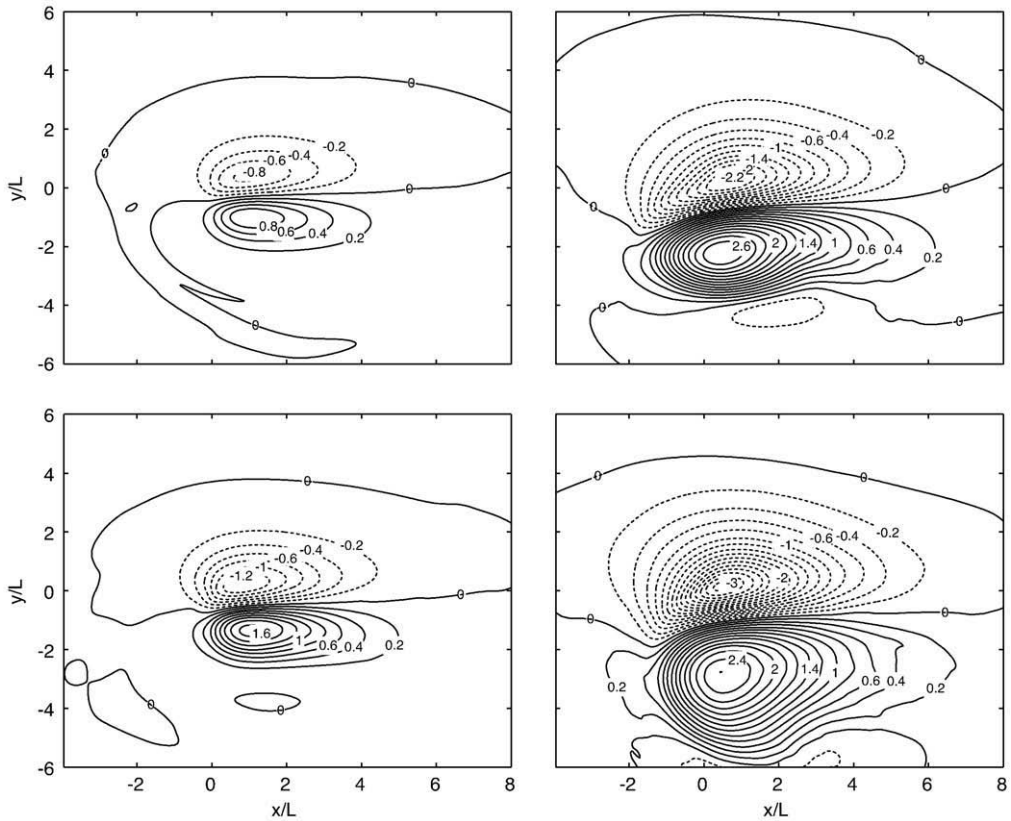

Fig. 7. The spatial structure of the disturbance in the mixed layer depth after 1 day (left panels) and 5 days (right panels) for wind forcing $\tau_{x0}=0.05$ N/m^2, $\Delta\tau_x=0.025$ N/m^2 (upper panels), and $\tau_{x0}=0.1$ N/m^2, $\Delta\tau_x=0.05$ N/m^2, (lower panels).

would provide a very strong forcing on the ecosystem in the vicinity of the wind farm during typical summer situations.

3.3. Results from a general circulation model

We end this section by showing results from some simple experiments carried out with the MITgcm general circulation model (Marshall et al., 1997a,b), which provides a non-linear as well as a full three-dimensional solution; we use the model in its hydrostatic mode although it has non-hydrostatic capability. To describe mixing in the upper ocean we apply the KPP turbulence mixing scheme (Large et al., 1994). We here assume that $L=5$ km and that the ocean is 20 m deep, and we apply no slip condition at the bottom (notably the KPP model will calculate the velocity at the first grid point according to a quadratic law). The temperature is 10 °C below −10 m and is 20 °C above −10 m, and we use a linear equation of state such that $\rho=\rho_0(1-\alpha T)$, where $\rho_0=1000$ kg m^{-3} and $\alpha=2\cdot10^{-4}$ K^{-1}. $f=1.2\cdot10^{-4}$ is taken as constant. The horizontal resolution is 200 m and the domain stretches from $x=-5L$ to $15L$ and from $y=-10L$ to $10L$, and we apply periodic boundary conditions. In the vertical we use 0.5 m resolution. The wind is applied instantaneously to an ocean at rest.

To visualize the ocean response to the wind forcing we define the following quantity

$$\Delta H_{\mathrm{ml}} = h_0 - \frac{1}{T_{\mathrm{U}}-T_{\mathrm{B}}}\int_{-H}^{0}(T-T_{\mathrm{B}})dz, \tag{8}$$

where $h_0=10$ m is the initial position of the thermocline, (T_{U}, T_{B})=(20,10) °C is the initial temperature of the upper and lower layers, respectively. The right-hand side of Eq. (6) will essentially measure the depth of the 10 °C isotherm, and subtracting this from the initial position of the 10 °C isotherm ΔH_{ml} will measure the amount of upwelling at a certain location.

The distributions of ΔH_{ml} after 1 resp. 5 days and a wind stress corresponding roughly to a wind speed 5 and 7.5 m/s (using a drag coefficient of $1.5\cdot10^{-3}$) are displayed in Fig. (7). The initial magnitude of the upwelling/downwelling is on the order of 0.8 m/day for the weak wind case, and is about 1.5 m/day for the strong wind case (Fig. 7a, c) in rough agreement with the theoretical estimates presented in Section 3.2 (i.e., 1 m/day and 2 m/day, respectively). However, after some time, say 2–3 days, the response becomes weaker, this weakening being most evident in the strong wind-forcing case. Most likely, non-linear effects become important as the amplitude of the disturbance grows. (The Rossby number (U/Lf) that measures the importance of non-linear terms relative to the Coriolis force is of order unity for $U=0.6$ m/s, furthermore the movements of the pycnocline are not negligible; we thus expect that the non-linear terms are important, but they do not dominate the system). Internal friction may be important but due to weak velocities in the lower layer we do not expect bottom friction to be important. Furthermore, it is clear from the numerical experiments that the shape of the disturbance changes and become wider with time.

Another striking property of the numerical model solution is that the response tends to become asymmetric with time, which is not predicted by the linear model. Notably, the depression of the pycnocline is wider and by smaller amplitude than the response in the upwelling sector. A possible explanation is that the upwelling leads to a cyclonic circulation while the downwelling generates an anti-cyclonic circulation. It is known in geophysical fluid dynamics that there are certain differences between cyclonic and anti-cyclonic eddies. However, an analysis of the dipole structure seen in these experiments is beyond the scope of the present study.

4. Results and discussion

The demand for electric power has stimulated many plans for constructing large off-shore wind-power plants. However, there have only been a few studies on the environmental impact of these wind farms on the oceanic environment; most available studies describe the direct effects of the wind mill constructions, noise and shadowing from the installations, and the possible influence of electric cables on the marine life. In this study we outline a possible environmental influence of the wind farms that, to our knowledge, has not previously been described in any detail in the scientific literature. More specifically, the wind farms may influence the wind pattern and hence force an upper ocean divergence. This will in turn influence the upwelling pattern, thereby changing, for instance, the temperature structure and availability of nutrients in the vicinity of the wind farm.

The basic oceanic response depends on the reduction in the wind stress at the sea surface, both in magnitude and the size of the affected area. From a literature review it appears that these quantities have not yet been studied in sufficiently detail to provide a reliable description of these features. Most studies of wind-farm influence on the wind focuses on the wind structure within the farm and how it will affect the efficiency of the wind farm. However, the far-reaching wind deficit and the wind stress at the sea surface have not been subjected to in substantial investigations. Thus, it is probably necessary with complementing studies of these issues before accurate estimates of the influence on the upper ocean physics can be established. Here, it should also be underlined that the size of the wind farm is a very important factor and that the oceanic response rapidly becomes much stronger when the size of the wind farm becomes larger than the internal radius of deformation.

Examples of how divergence of the wind causes upwelling in the ocean are when winds blow along a coast, over an island, or along the MIZ (Gill, 1982; Røed and O'Brian, 1983; Okkonen and Niebauer, 1995; Valiela, 1995; Botsford et al., 2003; Dugdale et al., 2006). With a wind-driven transport directed out from the coast the water that is transported out from the coast will be replaced by water from deeper layers through upwelling. These types of systems and the ecosystem response to the upwelling of nutrient rich, but also plankton poor, deep water have been studied extensively (Valiela, 1995; Botsford et al., 2003; Dugdale et al., 2006). However, there is an important difference between the upwelling forced along a coast and the type of upwelling that may be forced by large wind farms. In the coastal upwelling case, the presence of land implies that the ecosystem properties cannot be supplied from upstream condition; the wind-farm induced upwelling on the other hand, has an important upstream import of water that carries the properties of the ecosystem. The situation along the MIZ is probably more relevant but has

not been studied to the same degree; one difference here is that the position of MIZ change with time and reacts to the wind forcing while a wind farm has a fixed position.

We have not outlined the barotropic response in this study; this response is somewhat different but needs to be addressed. To the lowest order approximation the geostrophic balance inhabits vertical movements and the flow follows depth contours, or more specifically closed f/H contours. The basic steady state balance is characterized by a state where the net divergence over a closed f/H contour due to wind forcing is balanced by the net divergence induced by the Ekman layer at the bottom (Walin, 1972; Dewar, 1998; Nøst and Isachsen, 2003). It should be noted that the divergence of the wind field is generally small given the large size of atmospheric low-pressure systems. Accordingly, the wind tends to generate relatively weak barotropic signals around depth contours having small horizontal scales (say 100 km). The presence of a wind farm may create a substantial divergence of the wind field in the immediate vicinity of the wind farm. If the farm is placed close to a sloping bottom it is thus possible that the wind farm may provide a substantial additional forcing of the barotropic-current system in an ocean area. However, more studies using realistic systems are needed before it is possible to judge the strength of this forcing mechanism. Furthermore, if a substantial part of an enclosed or semi-enclosed ocean area is subject to wind farms there may be a measurable affect on the major basin-scale circulation and the associated pathways of nutrients.

Acknowledgements

Prof. Peter Lundberg provided valuable help on an early version of this manuscript. Two anonymous reviewers also provided insightful comments that improved the readability and impact of the manuscript. The model simulations were performed on the climate computing resource 'Tornado' operated by the National Supercomputer Centre at Linköping University. Tornado is funded with a grant from the Knut and Alice Wallenberg foundation.

References

Archer, C.L., Jacobson, M.Z., 2003. Spatial and temporal distributions of U.S. winds and wind power at 80 m derived from measurements. J. Geophys. Res. 108 (D9), 4289. doi:10.1029/2002JD002076.

Archer, C.L., Jacobson, M.Z., 2005. Evaluation of global wind power. J. Geophys. Res. 110, D12110. doi:10.1029/2004JD005462.

Baidya Roy, S., Pacala, S.W., 2004. Can large wind farms affect local meteorology? J. Geophys. Res. 109, D19101. doi:10.1029/2004JD004763.

Barthelmie, R.J., et al., 2003. Offshore wind turbine wakes measured by sodar. J. Atmos. Ocean. Technol. 20 (4), 466–477.

Botsford, L.W., Lawrence, C.A., Dever, E.P., Alan Hastings, A., Largier, J., 2003. Wind strength and biological productivity in upwelling systems: an idealized study. Fisheries Oceanogr. 12 (4–5), 245–259.

Branover, G.G., Vasilýev, A.S., Gleyzer, S.I., Tsinober, A.B., 1971. A study of the behavior of the eel in natural and artificial magnetic fields and an analysis of its reception mechanism. J. Ichthyol. 11 (4), 608–614.

Byrne, B.W., Houlsby, G.T., 2003. Foundations for offshore wind turbines. Phil. Trans. R. Soc. Lond. A 361, 2909–2930.

Christiansen, M.B., Hasager, C.B., 2005. Wake effects of large offshore wind farms identified from satellite SAR. Remote Sens. Environ. 98, 251–268.

Corten, G.P., Brand, A.J., 2004. Resource Decrease by Large Scale Wind Farming. Energy Research Centre of the Netherlands. ECN-RX-04-124.

Corten, G.P., Schaak, P., Hegberg, T., 2004. Velocity Profiles Measured Above a Scaled Windfarm. Energy Research Centre of the Netherlands. ECN-RX-04-123.

Dewar, W.K., 1998. Topography and barotropic transport control by bottom friction. J. Mar. Res. 56, 295–328.

Dugdale, R.C., Wilkerson, F.P., Hogue, V.E., Marchi, A., 2006. Nutrient controls on new production in the Bodega Bay, California, coastal upwelling plume. Deep-Sea Res. 53, 3049–3062.

Fennel, W., Johannessen, O.M., 1998. Wind forced oceanic responses near ice edges revisited. J. Mar. Syst. 14, 57–79.

Fennel, W., Lass, H.U., 2007. On the impact of wind curls on coastal currents. J. Mar. Syst. 68, 128–142.

Garthe, S., Hüppop, O., 2004. Scaling possible adverse effect of marine wind farms on seabirds: developing and applying a vulnerability index. J. Appl. Ecol. 41, 724–734.

Gill, A.E., 1982. Atmosphere–Ocean Dynamics. Academic Press, Inc., London. 662 pp.

Hasager, C.B., Barthelmie, R.J., Christiansen, M.B., Nielsen, M., Pryor, S.C., 2006. Quantifying offshore wind resources from satellite wind maps: study area the North Sea. Wind Energy 9, 63–74.

Hastings, M.C., Popper, A.N., 2005. Effects of Sound on Fish. http://www.dot.ca.gov/hq/env/bio/files/Effects_of_Sound_on_Fish23Aug05.pdf. Contract 43A0139 Task Order, 1, California Department of Transportation.

Hegberg, T., Corten, G.P., Eecen, P.J., 2004. Turbine Interaction in Large Offshore Wind Farms; Wind Tunnel Measurements. ECN-C-04-048, Energy Research Centre of the Netherlands.

Henderson, A.R., et al., 2003. Offshore wind energy in Europe — a review of the state-of-the-art. Wind Energy 6, 35–52. doi:10.1002/we.82.

Karlsen, H.E., 1992. Infrasound sensitivity in the plaice (*Pleuronectes platessa*). J. Exp. Biol. 171, 173–187.

Karlsen, H.E., Piddington, R.W., Enger, P.S., Sand, O., 2004. Infrasound initiates directional fast-start escape responses in juvenile roach *Rutilus rutilus*. J. Exp. Biol. 207, 4185–4193.

Keith, D.W., et al., 2004. The influence of large-scale wind power on global climate. Proc. Natl. Acad. Sci. 101, 16115–16120.

Knudsen, F.R., Enger, P.S., Sand, O., 1992. Awareness reaction and avoidance responce to sound in juvenile Atlantic salmon (*Salmo salar*). J. Fish Biol. 40, 523–534.

Kooijman, H.J.T., et al., 2003. Large scale offshore wind energy in the north sea. A Technology and Policy Perspective. Energy Research Centre of the Netherlands. ECN-RX-03-048.

Large, W.G., McWilliams, J.C., Doney, S.C., 1994. Oceanic vertical mixing: a review and a model with a nonlocal boundary layer parameterization. Rev. Geophys. 32 (4), 363–403.

Marshall, J., et al., 1997a. A finite-volume, incompressible Navier Stokes model for studies of the ocean on parallel computers. J. Geophys. Res. 102 (C3), 5753–5766.

Marshall, J., et al., 1997b. Hydrostatic, quasi-hydrostatic, and nonhydrostatic ocean modeling. J. Geophys. Res. 102 (C3), 5733–5752.

Nøst, O.A., Isachsen, P.E., 2003. The large-scale time-mean ocean circulation in the Nordic Seas and Arctic Ocean estimated from simplified dynamics. J. Mar. Res. 61 (2), 175–210.

Okkonen, S., Niebauer, H.J., 1995. Ocean circulation in the Bering Sea marginal Ice zone from Acoustic Doppler Current Profiler observations. Cont. Shelf Res. 15 (15), 1879–1902.

Pedlosky, J., 1987. Geophysical Fluid Dynamics. Springer-Verlag, New York. 710 pp.

Røed, L.P., O'Brian, J.J., 1983. A coupled ice ocean model of upwelling in the marginal ice zone. J. Geophys. Res. 88, 2863–2872.

Rooijmans, P., 2004. Impact of a large-scale offshore wind farm on meteorology. Ms Thesis, Utrecht University, Utrecht.

Sand, O., Karlsen, H.E., 1986. Detection of infrasound by the Atlantic cod. J. Exp. Biol. 125, 197–204.

Tucker, V.A., 1996a. A mathematical model of bird collisions with wind turbine rotors. J. Sol. Energy Eng. 118 (4), 253–262.

Tucker, V.A., 1996b. Using a collision model to design safer wind turbine rotors for birds. J. Sol. Energy Eng. 118 (4), 263–269.

Valiela, I., 1995. Marine Ecological Processes. Springer-verlag, New York. 686 pp.

Walin, G., 1972. On the hydrographic response to transient meteorological disturbances. Tellus 24, 1–18.

Wiggelinkhuizen, E.J., et al., 2006. WT-Bird: Bird Collision Recording for Offshore Wind Farms. Energy Research Centre of the Netherlands. ECN-RX-06-060.

Wiltschko, R., Wiltschko, W., 1995. Magnetic Orientation in Animals. Zoophysiology, vol. 33. Springer-Verlag. 297 pp.